Boundary Lubrication Properties of Materials with Expansive Freezing

E. A. Jagla

Centro Atómico Bariloche and Instituto Balseiro, Comisión Nacional de Energía Atómica, 8400 S.C. de Bariloche, Argentina

(Received 6 December 2001; published 3 June 2002)

We have performed molecular dynamics simulations of solid-solid contacts lubricated by a model fluid displaying many of the properties of water, particularly its expansive freezing. Near the region where expansive freezing occurs, the lubricating film remains fluid, and the friction force decreases linearly as the shear velocity is reduced. No sign of stick-slip motion is observed, even at the lowest velocities. We give a simple interpretation of these results, and suggest that, in general, good boundary lubrication properties will be found in the family of materials with expansive freezing.

DOI: 10.1103/PhysRevLett.88.245504 PACS numbers: 81.40.Pq, 05.10.–a, 46.55.+d

The understanding from a microscopic point of view of the tribological properties of materials in the boundary lubrication regime is of great importance for the technological development of new lubricants for new applications [1]. Micromechanical devices and high density magnetic storage media are just two examples where the detailed properties of the lubricants may affect in an important way the performance of the system. To attain low friction coefficients with lubricating films a few molecular layers thick is just the most obvious goal of lubricant design.

Fluid lubrication is a widespread strategy to reduce friction. However, it suffers of some limitations in the boundary regime [2], where the fluid is only a few molecular layers thick. Fluids have a general tendency to attain a solidlike structure when squeezed between two solid surfaces [2,3]. This confinement-induced solidification is responsible for microscopic stick-slip motion (SSM) [2] when the confining surfaces are sheared past each other. SSM in turn generates a finite friction force in the limit of low velocities, and then a nonzero friction coefficient. In fact, mechanisms that prevent SSM have been seen to reduce dramatically the friction force between the lubricated surfaces [4,5].

In the boundary regime, a lubricant composed of complex, branch chain molecules usually performs better than one formed by spherical, or single chain molecules, as the former does not readily arrange in a solidlike structure [6], and allows for a smooth shearing of the surfaces, in a state of very low friction. In addition, fluids with branch chain molecules have typically higher bulk viscosity than those with spherical, or single chain molecules. This justifies the experimentally observed (see Table 1 in Ref. [6]) negative correlation existing between bulk viscosity and friction coefficient under boundary lubrication conditions.

Water is a noteworthy exception to this rule [6]. The water molecule is a small, almost spherical particle, and the viscosity of water is very low. However, carefully controlled experiments using the surface force apparatus show that water is an excellent boundary lubricant at a microscopic scale [7–9]. In fact, the friction coefficient between two water lubricated, atomically flat mica surfaces was found [6,7] to be around 0.01, in the range of the lowest values obtained with other fluids in the boundary regime. The reason for the anomalously good lubrication properties of water has not been addressed in detail. In this paper we show, by studying a model system, that the good lubrication properties of water can be associated to its expansive freezing, and that good boundary lubricants can be fetched, in general, within the class of materials having this property.

Many of the anomalous properties of water (and tetrahedrally coordinated liquids in general [10]) have been recently systematized by the use of a model system of spherical particles interacting through a soft-core potential [11–13]. Its main characteristic is the existence of two stable relative distances between particles, as a function of the applied pressure. It has been suggested that these two distances are realized in water owing to two distinct arrangements of hydrogen bonds [14]. We use one such model [11] to simulate a lubricant film. The interaction potential as a function of the interparticle distance r has a strict hard core at a distance $r = \sigma$ and a repulsive ramp extending from σ to $\alpha\sigma$ ($\alpha > 1$, $\alpha = 1.5$ hereafter), in which the potential energy changes linearly from ε to zero. Natural units for this problem are the length σ, the energy ε, and the mass of the particles m, from which a time scale $\tau \equiv \sqrt{m\sigma^2/\varepsilon}$ is defined.

The bulk system freezes into a closed packed lattice with lattice parameter $\sim\alpha\sigma$ at low temperatures and low pressures. The melting curve of this crystalline structure was determined previously by Monte Carlo simulations [11], and is reproduced in Fig. 1(a) for completeness. The melting temperature increases as a function of pressure at the lowest values of P and T, consistent with the fact that in this region particles behave as hard spheres of radius $\alpha\sigma/2$. At higher pressures, the melting line reenters toward lower temperatures as neighbor particles can get closer than $\alpha\sigma$ [15]. Other crystalline structures exist at higher pressures [15,16].

The geometrical arrangement we use for the simulations is similar to that used in Refs. [17,18], and is sketched in Fig. 1(b). It qualitatively models the configuration used in the surface force apparatus [1]. Two opposing pieces of crystalline fcc solids exposing (111) faces are lubricated by

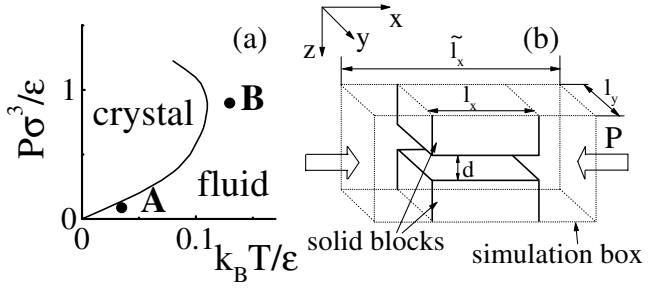

FIG. 1. (a) The melting line of the low pressure bulk crystalline structure of our model fluid. The system has other stable crystalline structures at higher pressures, not indicated here. The points **A** and **B** are those simulated, with the results shown in Figs. 2 and 3, respectively. (b) A sketch of the geometrical configuration used in the simulations. Fluid particles fill up the simulation box. Crystal structure of solid blocks is not shown here. The external hydrostatic pressure P is indicated.

our model system. Particles within the solids are assumed to be fixed to their lattice positions, and the interactions between particles of the fluid and those of the solids are taken equal to the intrafluid interactions. The lattice parameter of the solid blocks a_0 is chosen for each pressure as that of the bulk solid at the melting temperature. This is not a crucial choice, and is made only to avoid introducing a bias between the different simulated points. The lubricant particles within the gap between the solids are at dynamic equilibrium with lubricant particles outside the gap. For the static (no shear) simulations, periodic boundary conditions are applied in the three directions. The solid blocks are of finite size l_x in the x direction, and extend over the whole length of the simulation cell l_y in the y direction. The size of the simulation box in the x direction $\tilde{l}_x$ is substantially larger than l_x, allowing to reach a dynamical equilibrium between the lubricant inside the gap, and the bulk fluid outside it. $\tilde{l}_x$ is allowed to change according to the value of a hydrostatic external pressure P. Real fluids always possess some attraction between particles, which we have not included. It is known, however, that the attraction between particles (both fluid-fluid and fluid-solid) in the van der Waals limit can be readily included in the results obtained without attraction by the renormalization of the external pressure [11]. Our hydrostatic pressure P accounts for the attraction between particles in the van der Waals limit, this attraction being of the same strength between fluid-fluid particles and fluid-solid ones. Other cases remain to be studied.

We have chosen $l_x \times l_y$ equal to $15 \times 15\sigma^2$. Each lubricant monolayer within the gap has about 110 particles, and the total number of fluid particles simulated is 800. We have performed checks with systems of up to 3500 fluid particles and $l_x \times l_y$ equal to $30 \times 30\sigma^2$, to assure that size effects do not spoil the results. We simulated systems at points **A** and **B**, indicated in Fig. 1 ($P_A = 0.1\varepsilon/\sigma^3$, $T_A = 0.035\varepsilon/k_B, P_B = 0.9\varepsilon/\sigma^3, T_B = 0.13\varepsilon/k_B$). We calculated the normal force exerted by the lubricant — the solvation force — and studied the structure of the film as a function of the distance d between the two solid surfaces. In Fig. 2 we show results at point **A**, where the system behaves basically as a hard sphere system. When d is only a few molecular radii, the solvation force per unit area F_s shows a well-known [1,17–22] oscillatory behavior (centered at the value of the hydrostatic pressure P) associated to the layering of the fluid. The number of particles inside the gap n_p (which is normalized to one for a full layer of particles) has a staircaselike structure, remaining approximately constant as F_s increases (we describe the process as d is reduced), and jumping down coincidentally with the reduction of F_s, when a layer of lubricant is squeezed out of the gap. Gray regions in Fig. 2 indicate precisely these squeezing-out regions, where the number of layers is changing. We measure the horizontal order within the lubricant through the structure factor f of the layers adjacent to the solids (calculated at $|k| = 4\pi/a_0$), and the two-dimensional (horizontal) diffusivity of particles in the gap D. Within a plateau of n_p, f increases and D decreases as the film is compressed, indicating that the film becomes more structured as F_s increases. In the squeezing-out regions (the gray regions), f drops and D maximizes, indicating that the film becomes less structured and more fluid. This whole picture

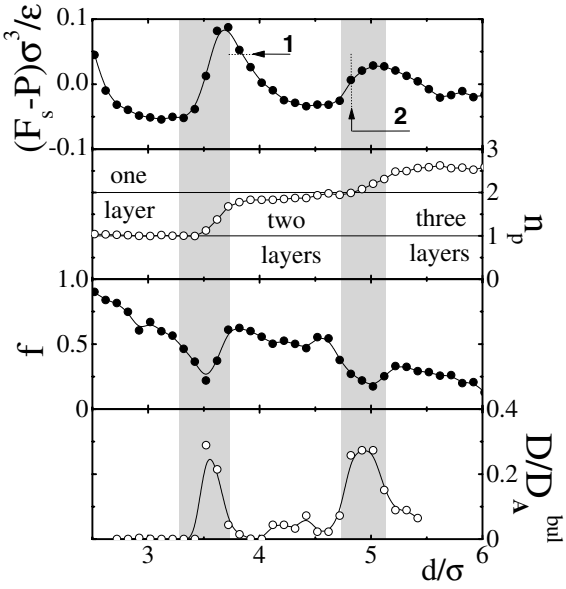

FIG. 2. Structure of the lubricant film at point **A** of the phase diagram as a function of the gap width d. We show the equilibrium values of the solvation force F_s, the number of particles in the gap n_p (normalized to a full layer of particles), the structure factor f of the lubricant layers adjacent to the solids, and the horizontal diffusivity D of particles in the gap (D is measured relative to the bulk three-dimensional value at point **A**, $D_A^{\text{bulk}} \simeq 0.012\sigma^2/\tau$). In the gray regions, there are drops of F_s, associated with the expulsion of a whole lubricant layer, as seen by the evolution of n_p. This expulsion is correlated with a decrease of f and an increase of D, which indicates that the film becomes more disordered, or fluidlike, in these regions.

is consistent with previous studies [17,18], and it can also be given a straightforward interpretation: If we assimilate F_s to a sort of local pressure in the film, the increasing of order as F_s increases is consistent with the fact that for the bulk material positional order increases and diffusivity decreases with the applied pressure. When a layer is being squeezed out, more space is available to the remaining particles that then attain a more fluid configuration.

Results are shown in Fig. 3 near the region where expansive freezing occurs (point **B** in Fig. 1). F_s shows the same oscillating behavior as before. However, the structure of the film is now qualitatively different. The film remains in a liquidlike state as F_s increases (as seen from the values of f and D). This occurs because particles, being at distance $\sim 1.5\sigma$ from their neighbors, can go closer (up to distance $\sim\sigma$) upon a reduction of d, without generating a higher degree of order in the system. Only after F_s decreases, the film becomes more solidlike (with higher f and lower D). This is also consistent with the fact that this kind of model (as well as real water [23]) is known to have a range of pressure in which diffusivity increases as pressure increases [24]. Close to this region [which occurs near the maximum of the $P(T)$ melting line], a positive correlation between the values of F_s and D can be expected.

The inverted alternate at point **B** of liquidlike and solidlike structure of the film upon compression represents a crucial difference from an experimental point of view, since typically a condition of constant load is applied to the contact. For stability reasons, this external load will be sustained by a lubricating film at a point with a negative derivative of F_s with respect to d, namely, it will be a solidlike film at point **A**, and a liquidlike film at point **B**. As we will see, this difference has profound consequences in the lubricating properties of the system.

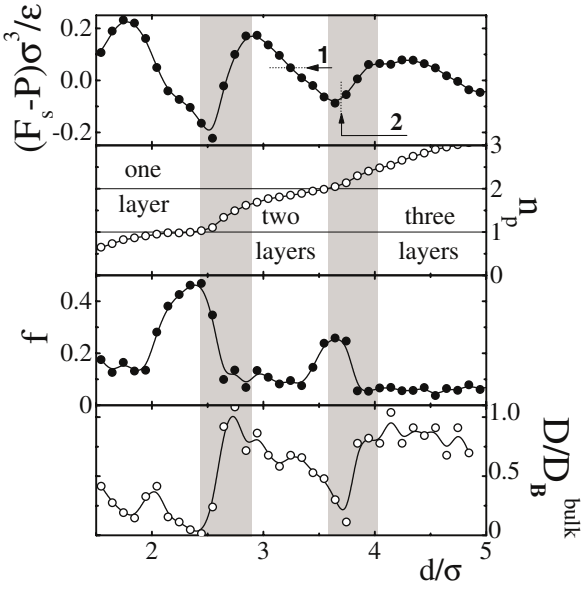

FIG. 3. Same as Fig. 2 but at point **B** of the phase diagram. The trends for F_s and n_p are the same as those seen in Fig. 2, but now the expulsion of a lubricant layer (within the gray regions) produces an ordering of the film, as seen from the increase of f and the decrease of D ($D_B^{\text{bulk}} \simeq 0.022\sigma^2/\tau$).

Shearing simulations were performed in the same geometry as that used for the previous calculations, but now the upper solid block (which is now allowed to move in the y direction) is given a mass M ($M = 450m$), and is attached to a horizontal spring (spring constant $k = 0.45\varepsilon/\sigma^2$) whose free end is moved in the y direction at a constant velocity v (see also [4]). An external load per unit area L of $0.05\varepsilon/\sigma^3$ in excess of the hydrostatic pressure P within the lubricant is applied to the block along the z direction, and the distance d is allowed to change dynamically during the simulation.

Both at points **A** and **B** a two-layer thick film was first stabilized (corresponding approximately to points labeled **1** in Figs. 2 and 3, we will refer to these conditions as $\mathbf{A}_1$ and $\mathbf{B}_1$, respectively). The friction force F_f as a function of time was calculated for different shear velocities, and the results are shown in the main panel of Fig. 4. We show the time dependence of F_f for the points of lowest velocities in the bottom part of Fig. 4. At $\mathbf{A}_1$, the mean friction

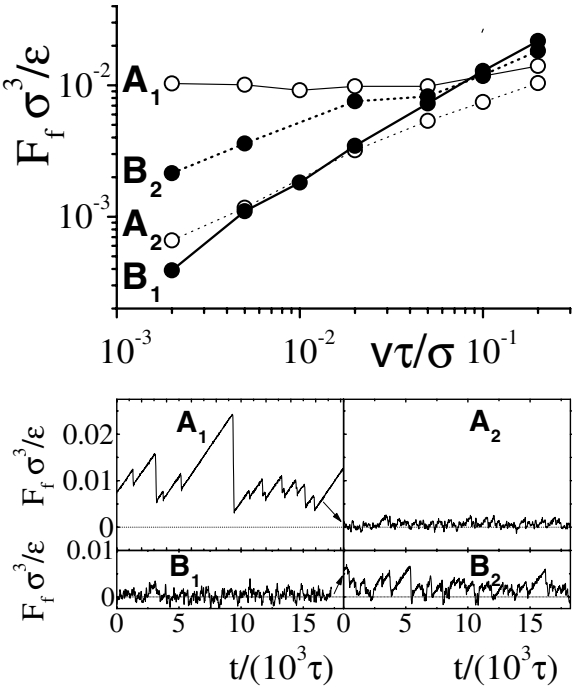

FIG. 4. Top: friction force per unit area F_f as a function of shear velocity for points **A** and **B** of the phase diagram. Continuous lines are results at a constant load L of $0.05\varepsilon/\sigma^3$ in excess of the hydrostatic pressure (points labeled **1** in Figs. 2 and 3). Dotted lines are the results of simulations at constant d, chosen in such a way that now the film is quasiliquid at $\mathbf{A}_2$, and quasisolid at $\mathbf{B}_2$ (point labeled **2** in Figs. 2 and 3). Bottom: F_f as a function of time for the points of lowest velocities, displaying SSM at $\mathbf{A}_1$ (for which F_f goes to a finite value as v is reduced) and uniform motion at $\mathbf{B}_1$ (for which F_f decreases linearly as v is reduced). SSM is strongly suppressed at $\mathbf{A}_2$ as compared to $\mathbf{A}_1$, and reappears in $\mathbf{B}_2$, as compared to $\mathbf{B}_1$.

force goes to a constant when v is reduced, as SSM sets in, around $v \sim 0.05\sigma/\tau$, which reproduces previous results in related models [4,25]. The limiting value of the friction force corresponds in our case to a friction coefficient $\mu \simeq 0.2$. At $\mathbf{B}_1$ the friction force decreases linearly as v is reduced. No SSM is observed in this case [26]. This is consistent with the fluidity of the lubricant even in this highly confined geometry, a fact recently observed in water [8]. The linear dependence of the friction force $F_f(v)$ on v can be used to estimate an effective viscosity η^{eff} for the film as $\eta^{\text{eff}} \equiv F_f(v)d/v \simeq 0.7\varepsilon\tau/\sigma^3$, which is within 3 times the bulk value obtained by an independent measurement of the bulk single particle diffusivity ($D_B^{\text{bulk}} \simeq 0.022\sigma^2/\tau$) and use of the Stokes-Einstein relation. This remarkable fact is to be compared with the finding that viscosity of water confined to molecular thicknesses has been shown [8] to be no more than a few times the bulk value, and it can also be traced back to the high value of diffusivity obtained in the static calculation at point **1** in Fig. 3, which is close to the bulk value.

Since temperature and pressure are different at points **A** and **B**, an additional check of the proposed scenario is desirable. Therefore, we did additional simulations in which the behavior is expected to be reversed: We performed fixed d simulations at values $d = 4.8\sigma$ at **A**, and $d = 3.7\sigma$ at **B** (labeled **2** in Figs. 2 and 3, we will refer to these conditions as $\mathbf{A}_2$ and $\mathbf{B}_2$, respectively. Note that constant load simulations at these values of d would be unstable). We have obtained, in fact, a big reduction of the friction force at $\mathbf{A}_2$ with respect to $\mathbf{A}_1$, with no SSM detectable even at the lowest velocities (see bottom of Fig. 4), and an increase of the friction force at $\mathbf{B}_2$ with respect to $\mathbf{B}_1$, where now SSM becomes observable at the lowest velocities.

In summary, we have shown that materials with expansive freezing are expected to have good boundary lubrication capabilities, essentially due to the fact that they do not show a strong tendency to solidify as they are squeezed. This finding provides a novel strategy in the design of materials for boundary lubrication. At the same time, our results give a qualitative explanation for the good lubrication properties and low viscosity of very thin films of water. They also predict that experiments performed at constant d, at the squeeze-out points (such as $\mathbf{B}_2$) will produce larger friction forces than constant load experiments, contrary to what is expected in normal fluids. Similar results are likely to be obtained in other materials with expansive freezing.

I thank C. A. Balseiro and E. Tosatti for critical reading of the manuscript, and A. Borsinger for technical assistance. This work was financially supported by CONICET, Argentina. Partial support by Fundación Antorchas (Argentina) and Italian Contracts No. INFM/PRA NANORUB and No. MIUR/COFIN is also acknowledged.

[1] B. Brushan, J. N. Israelachvili, and U. Landman, Nature (London) **374**, 607 (1995).
[2] B. N. J. Persson, *Sliding Friction: Physical Principles and Applications* (Springer, Heidelberg, 1998).
[3] J. Klein and E. Kumacheva, J. Chem. Phys. **108**, 6996 (1998).
[4] J. Gao, W. D. Luedtke, and U. Landman, J. Phys. Chem. B **102**, 5033 (1998).
[5] M. Heuberger, C. Drummond, and J. N. Israelachvili, J. Phys. Chem. B **102**, 5038 (1998).
[6] J. N. Israelachvili, Surf. Sci. Rep. **14**, 109 (1992).
[7] A. M. Homola, J. N. Israelachvili, M. L. Gee, and P. M. McGuiggan, J. Tribol. **111**, 675 (1989).
[8] U. Raviv, P. Laurat, and J. Klein, Nature (London) **413**, 51 (2001).
[9] S. E. Grillo and J. E. Field, Eur. Phys. J. B **13**, 405 (2000).
[10] C. A. Angell, R. D. Bressel, M. Hemmati, E. J. Sare, and J. C. Tucker, Phys. Chem. Chem. Phys. **2**, 1559 (2000).
[11] E. A. Jagla, J. Chem. Phys. **111**, 8980 (1999).
[12] A. Scala, M. R. Sadr-Lahijany, N. Giovambattista, S. V. Buldyrev, and H. E. Stanley, Phys. Rev. E **63**, 041202 (2001).
[13] G. Franzese, G. Malescio, A. Skibinsky, S. V. Buldyrev, and H. E. Stanley, Nature (London) **409**, 692 (2001).
[14] O. Mishima and H. E. Stanley, Nature (London) **396**, 329 (1998).
[15] E. A. Jagla, Phys. Rev. E **58**, 1478 (1998).
[16] E. A. Jagla, J. Chem. Phys. **110**, 451 (1999).
[17] J. Gao, W. D. Luedtke, and U. Landman, J. Phys. Chem. B **101**, 4013 (1997).
[18] J. Gao, W. D. Luedtke, and U. Landman, Phys. Rev. Lett. **79**, 705 (1997).
[19] M. L. Gee, P. M. McGuiggan, and J. N. Israelachvili, J. Chem. Phys. **93**, 1895 (1990).
[20] I. K. Snook and W. van Megen, J. Chem. Phys. **72**, 2907 (1980).
[21] S. K. Das, M. M. Sharma, and R. S. Schechter, J. Phys. Chem. **100**, 7122 (1996).
[22] Y. Wang, K. Hill, and J. G. Harris, J. Chem. Phys. **100**, 3276 (1994).
[23] F. X. Prielmeier, E. W. Lang, R. J. Speedy, and H.-D. Ludemann, Phys. Rev. Lett. **59**, 1128 (1987).
[24] E. A. Jagla, Mol. Phys. **99**, 753 (2001).
[25] P. A. Thompson and M. O. Robbins, Science **250**, 792 (1990).
[26] From the shear simulations, we cannot rule out the existence of SSM at lower velocities, but from the results in Fig. 4 an upper bound of $\sim$0.01 for the friction coefficient μ at $\mathbf{B}_1$ is obtained, namely, 20 times lower than for $\mathbf{A}_1$.